



## ASME Accepted Manuscript Repository

### Institutional Repository Cover Sheet

University of Delaware Library Open Access Team

---

A High-Consolidation Electron Beam-Curing Process for Manufacturing Three-Dimensional  
ASME Paper Title: Advanced Thermoset Composites

---

Authors: Robert H. Rizzolo, Daniel F. Walczyk, Daniel Montoney, Pavel Simacek, Md Rashef Mahbub

---

ASME Journal Title: Journal of Manufacturing Science and Engineering

---

Volume/Issue Volume 144, Issue 12

Date of Publication (VOR\* Online) July 27, 2022

<https://asmedigitalcollection.asme.org/manufacturingscience/article-abstract/144/12/121001/1141850/A-High-Consolidation-Electron-Beam-Curing-Proces>

DOI: <https://doi.org/10.1115/1.4054871>

---

\*VOR (version of record)

# A High-Consolidation Electron Beam-Curing Process for Manufacturing 3-D Advanced Thermoset Composites

Robert H. Rizzolo<sup>a</sup>, Daniel F. Walczyk<sup>a\*</sup>, Daniel Montoney<sup>b</sup>, Pavel Simacek<sup>c</sup>, Md Rashef Mahbub<sup>a</sup>

<sup>a</sup>Department of Mechanical, Aerospace & Nuclear Engineering  
Rensselaer Polytechnic Institute  
110 Eighth Street  
Troy, New York 12180 USA  
Robert.Rizzolo@gmail.com; walczd@rpi.edu; mahbum@rpi.edu

<sup>c</sup>Rapid Cure Technologies, Inc.  
7030 Fly Road  
East Syracuse, New York 13057 USA  
dan@rapidcuretechnologies.com

<sup>c</sup>Center for Composite Materials  
University of Delaware  
101 Academy Street  
Newark, Delaware 19716  
psimacek@udel.edu

\*Corresponding Author

## Abstract

This paper describes application of a new manufacturing process for low-cost and rapid consolidation and curing of advanced thermoset composites that avoids the use of expensive prepreg, autoclaving, and thermally induced curing. The process, called VIPE, uses a novel tooling design that combines vacuum infusion (VI) of a dry preform with resin, a rigidly backed pressure focusing layer (P) made of an elastomer to consolidate the wet preform with uniform pressure, and high-energy electron beam curing (E). A VIPE tool is engineered and fabricated to manufacture 3-D laminate bicycle seats comprised of woven carbon fiber textile and an electron beam-curable epoxy acrylate. Details of the tooling design discussed include CFD simulation of the vacuum infusion, iterative structural FEA to synthesize the pressure focusing layer, structural FEA to design the top mold made of a composite sandwich structure for electron beam transparency, and Monte Carlo electron absorption simulations to specify the e-beam energy level. Ten parts are fabricated using the matched tool (bottom aluminum mold covered with silicone layer, top mold with carbon/epoxy skins separated by foam core) after the dry textile preform contained within is infused with resin, the tool halves are clamped under load, and a 3.0 MeV e-beam machine bombards the tool for less than one minute. Part thickness, part stiffness, surface roughness, and fiber and void volume fractions measurements show that aerospace-quality parts with low cycle times are achievable, although there is high variability due to the small number of replicates and need for process optimization.

## 1. Introduction

The worldwide market for advanced thermoset composites is large and continues to grow due to the need for advanced materials with high specific strength and stiffness, and chemical and temperature resistance by various end user industries (e.g., transportation, aerospace, pipe and tank, construction, wind energy, and consumer goods). One market research report [1] estimates that the market will reach \$77 billion (USD) by 2027. Thermoset composites industry trends related to materials and manufacturing that are driven by the market growth include lowering material costs, faster processing and rapid cure resin systems (especially for automotive applications), bio-based resins, reduced consumables, and fire resistance.

The research discussed herein builds upon prior work on processing technology and practice for advanced thermoset composites that has the potential to significantly reduce cycle time, consumables used, and material cost by allowing in situ resin infusion, consolidation without an autoclave, and rapid curing. The new technology – a combination of vacuum infusion (VI) of dry fiber preforms with liquid thermoset resin in place of prepreg, the use of Pressure Focusing Layer™ (P) tooling to consolidate composite layups<sup>1</sup>, and electron beam curing (E) of the resin – is identified by the acronym VIPE. Vacuum infusion eliminates the need for expensive prepreg, and pressure focusing layer tooling combined with electron beam curing eliminates the need for autoclaving. As shown in Figure 1, the VIPE process involves the following steps.

- 1) Place a dry composite preform onto a solid bottom mold (e.g., aluminum) covered with a specially engineered variable-thickness pressure focusing layer (silicone rubber mask) which is backed by a matching top mold made from a composite sandwich structure that allows for electron beam irradiation.
- 2) Assemble and hold two mold halves together to seal the preform cavity, and then infuse the preform and or space between the preform with an electron beam-curing resin by pulling vacuum.
- 3) Clamp the two mold halves together with a specific load to compress the pressure focusing layer so that a uniform consolidation pressure is applied to the entire surface of the resin-infused composite layup. Tighten clamping bolts along the outside perimeter of the mold to maintain the consolidation pressure.
- 4) Irradiate the part from the top mold side with a high-intensity electron beam to completely cure the part. Unclamp mold halves to retrieve the cured composite part.

This paper discusses the application of VIPE to a 3-D laminate part shape (bicycle seat) along with technological issues, model-based design process, tooling design, and materials.

---

<sup>1</sup>Pressure Focusing Layer (PFL) process has been trademarked by Vistex Composites, LLC, Schenectady, NY, USA.

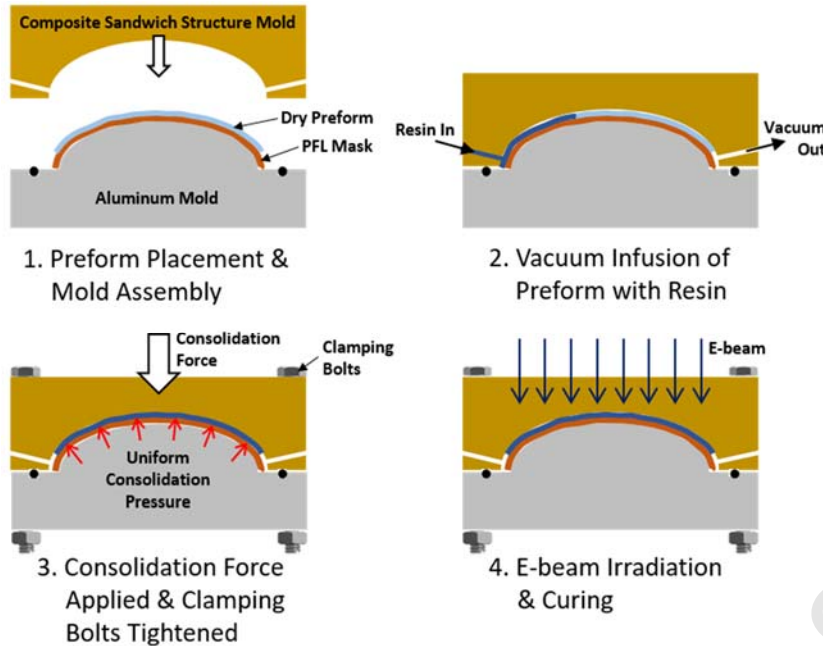


Figure 1. Schematic of the VIPE process

## 2. Background

Prior work related to the three basic technologies comprising the VIPE process – electron beam curing, PFL tooling, and vacuum infusion – are covered in this section.

**Electron Beam Curing.** Electron Beam (EB) curing of advanced composites, which can be traced back to the late 1970's in France according to Beziere et al. [2], has been compared to other curing processes (primarily thermal) by numerous research groups. Crasto et al. [3] tested resin properties of a thermal cure epoxy for composites with a EB-cure equivalent and found that  $T_g$  and mechanical properties were significantly lower for the latter. They recommended more effort in formulating resins and sizings to take advantage of the inherent processing advantages of EB-cure resins. Lopata et al. [4] reviewed early chemistry work related to EB-curable epoxies and summarized the advantages of these resins over thermally cured counterparts. Glauser et al. [5] compared EB-, UV-, and thermal-curing of acrylate and methacrylate resins and deemed EB-curing the best method due to higher  $T_g$  values, better mechanical properties, significantly shorter processing time, and deeper penetration. Berejka and Eberle [6] reviewed the state of the art in EB curing of composites in North America and concluded that EB-cure resin properties are approaching those of analogous thermally cured resins, and cost reductions of 10-50% are possible due to rapid cure and lower energy consumption. Lopata and Sidwell [7] provide a comprehensive summary on the state of EB composites processing and repair up to the early 2000s. Stated advantages of EB resin systems include room-temperature storage, ability to debulk/consolidate at room temperature, and the ability to use inexpensive tooling including low-density foam. Disadvantages are the limited availability of qualified EB resins, UV and near-UV light sensitivity, chemical incompatibility of some existing consumables used for thermal cure systems, and lack of fiber sizing and primers designed for EB resins. EB curing was shown to provide better adhesion between vinyl ester resin and carbon fibers as compared to chemical curing by Zsigmond et al. [8]. Nishitsuji et al. [9] describes the advantages of EB-cured thermoset resins over their thermally cured counterparts. Their research showed that an epoxy resin with cationic initiator cured by EB irradiation has a higher  $T_g$  (20%) and order-of-

magnitude shorter cure time. Vautard et al. [10] found that the interfacial shear strength of a carbon/diacrylate resin composite cured with EB was significantly lower than for one that was thermally cured unless a post-cure is performed. EB curing alone did not create the same interface interactions as thermal curing. The process has been applied to composite boat hull construction [11] and aerospace parts [12].

Several research groups have been successful at improving the mechanical properties of EB-cured advanced composites through better resin chemistries and fiber treatments. Jianwen et al. [13] demonstrated EB curing of an epoxy resin for advanced composites that has high temperature resistance. Coqueret et al. [14] reviewed recent advances in the improvement of free radical and cationic type thermoset resins for composites and presents a more advanced curing kinetics model. Vautard et al. [15] designed a reactive sizing for a carbon fiber/acrylate composite system cured by EB that provides the same interlaminar shear strength to an equivalent thermally cured system. More recently, Zhang et al. [16] demonstrated improved carbon fiber/epoxy interfacial shear strength and interlaminar shear strength by irradiating the carbon fibers before impregnation with microwaves.

Several researchers have investigated the effect of process improvements on EB-cured composites. Goodman et al. [17] demonstrated low-energy EB curing of prepreg using an AFP deposition head. Fengmei et al. [18] and Sui et al. [19] investigated the effects of process parameters on the degree of cure and properties of EB-cured epoxies. Abliz et al. [20] has demonstrated carbon/epoxy prepreg curing prior to AFP using low-energy EB irradiation (up to 150 keV). They found that pre-curing did not allow good prepreg consolidation and resin flow as compared to high-energy EB or thermal curing. It also required a post thermal cure to achieve acceptable properties. The research described in this paper focuses on additional process improvements, namely, combining resin infusion and out-of-autoclave consolidation with EB curing.

Applying uniform consolidation pressure while curing is arguably the most important step for the production of high quality composite parts, as it largely determines the part's final fiber volume and void volume fractions, which one wants to maximize and minimize, respectively. Autoclaving, the industry standard for composite part consolidation/curing, generally involves using pressurized and heated inert gas (e.g., nitrogen) to apply a high, uniform consolidation pressure and temperature on the part (usually in a vacuum bag) while avoiding oxidation or combustion issues. The pressure and temperature buildup takes time, causing a bottleneck in the manufacturing process. While very effective at producing high quality parts, autoclaves are also very inefficient from both a time and energy standpoint. This has resulted in a trend within the composites industry towards the development of out-of-autoclave (OOA) technologies.

*Pressure Focusing Layer Process.* The Pressure Focusing Layer (PFL) process is a patented OOA technology [21] commercialized by Vistex Composites, LLC [22] that serves as a low-cost (both fixed and variable), low-energy, and reduced-cycle time alternative to autoclaving for consolidation and curing advanced composites. The process uses a temperature-controlled curing mold paired with a compression mold covered by a variable-thickness rubber mask (typically high-temperature silicone) to sandwich a prepreg layup. The mold set is specially engineered using computational modeling and optimization so that: (1) when a particular load is applied, the compressed rubber mask applies a uniform pressure over the entire part surface; and (2) uniform curing temperature is maintained. Walczyk et al. [23-25] demonstrated the PFL process for increasingly complex and larger part shapes, and Malek et al. [26] investigated the properties of silicone masks subject to repeated loading/unloading cycles.

*Evolution of the VIPE Process:* Vacuum infusion, a well known and widely used process for impregnating dry fiber preforms with resin using differential pressure, was combined with the PFL process to successfully impregnate dry fiber preforms then consolidate and thermally cure flat carbon fiber/epoxy [27] and cellulose textile/epoxy [28] laminate parts. This research showed that PFL was not limited to just prepreg layups. Rizzolo et al. [29] was the first to add rapid curing of the thermoset matrix through EB irradiation after the resin infusion step, thereby demonstrating all three processes that comprise VIPE for flat laminate parts. The process is extended to 3-D parts in this paper.

### 3. VIPE Process and Tooling Design

The 3-D part shape chosen for this VIPE investigation was a simple bicycle seat, shown in Figure 2, made from a carbon/epoxy material system, that has curved peripheral edges and both steep and gentle sloping areas. Maximum dimensions of the bicycle seat are 31 mm high  $\times$  140 mm wide  $\times$  240 mm long. A flattened cut-out shape for the fiber preforms were developed using a built-in Solidworks flattening tool, as well as an iterative “cut-and-fill” test with an additively manufactured mold. The chosen reinforcement was Fibre Glast 530, a 3K plain weave carbon fiber fabric with 0.305 mm nominal thickness. The matrix used was the same as the flat laminate part experiments [29] – Rapid Cure Technologies 2005-102-1 resin, an epoxy acrylate with cationic cure chemistry, recommended cure dose level of 40-80 kGy, and room temperature viscosity of 250-300 cP (suitable for vacuum infusion). Bicycle seats were made with both four 4 plies (1.22 mm total thickness) and five plies (1.53 mm total) with [0<sub>4</sub>] and [0<sub>5</sub>] layups, respectively.

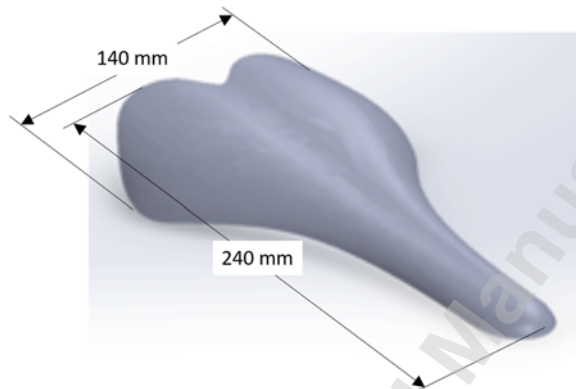


Figure 2. Bicycle seat geometry with dimensions shown.

Process and tooling requirements for the bicycle seat pertain to vacuum infusion, consolidation, and curing. For vacuum infusion, the goal is one resin inlet and one vacuum outlet that are optimally positioned to allow for full impregnation, minimized fill time, and provide little or no interference with the electron beam during curing. After full infusion, a uniform consolidation pressure of 0.69 MPa (100 psi) is required. Additional requirements related to the PFL method include a rigid bottom mold, complementary silicone rubber mask, and a sufficiently rigid top mold that does not significantly attenuate the electron beam. Finally, the radiation dose level needed for curing is provided by the manufacturer, but the minimum EB energy level required to avoid attenuation through the top mold and composite part must be defined.

#### 3.1 Vacuum Infusion Configuration

A major problem with flat panel manufacturing using the VIPE process [29] was insufficient resin wet-out during vacuum infusion due to the resin inlet and vacuum venting ports located at opposite sides of the panel for uniaxial flow. Gaps between the mold and preform along the long edges led to resin racetracking and dry spots in the center of the preform unless infusion was slowed significantly (i.e. using lower pressure).

To address this issue with a more complicated 3D geometry, Computational Fluid Dynamics (CFD) modeling of vacuum infusion was performed using the *Liquid Injection Molding Simulation* (LIMS) software with a mesh created in *Gmsh*, a three-dimensional finite element mesh generator. Inlet and venting ports are ideally located along the part perimeter so that porting hardware in no way interferes with part curing during EB irradiation, although this may be difficult to achieve in practice. Four different exterior inlet and port configurations (#1-4), as shown in Figure 3, were considered for the 4-ply preform with 0.1 mm (narrow) and 0.5 mm (wide) gaps that simulate racetracking (i.e. uniform gap between preform and perimeter of mold cavity that allows resin to rapidly flow). A 0.1 and 0.5 mm gaps represent tight and loose preform fits. If we solve Darcy's Law for 1D flow, the relationship between the distance the resin flow front has travelled,  $x$ , through a porous dry composite preform versus time,  $t$  is

$$t = \int_0^t dt = \int_0^x \left( \frac{\mu x}{Kp} \right) dx = \frac{\mu x^2}{2Kp} \quad (1)$$

where  $\mu$  = viscosity of the polymer resin,  $K$  = in-plane permeability of the dry fiber preform, and  $p$  = the differential pressure applied. Rearranging Eqn. 1 allows us to solve for  $K$  in terms of experimental constants  $\mu$  and  $p$ , and the slope of  $x^2$  vs.  $t$ ,

$$K = \left( \frac{x^2}{t} \right) \left( \frac{\mu}{2p} \right) \quad (2)$$

Permeability for the resin/preform layout combination was determined to be  $K = 1.5 \times 10^{-12} \text{ m}^2$  based on a single unidirectional vacuum infusion test (Figure 4) and room-temperature viscosity of  $\mu = 350 \text{ cP}$  for the resin measured using a Brookfield viscometer. These values for  $K$  and  $\mu$  were used for all LIMS simulations. For example, a simulation of flow front vs. time for port combination #1 is shown in Figure 5(a), and maximum fill time and final infusion outcome for each combination are provided in Table 1. Part configurations #1-4 suffered from incomplete filling except for #1 and #3 with the 0.1 mm gap, although filling times were roughly 19 min and 9 min, respectively.

To reduce fill time (and manufacturing cycle time) even further, a single vent located in the part interior near the high point of the mold and inlets along the perimeter was investigated. Interior venting is not ideal, as previously mentioned, but a simple vent capping strategy would be used to minimize any EB attenuation. Furthermore, a large gap (1 and 5 mm) was included around the perimeter to act as a manifold and provide a convergent resin flow strategy. Two different exterior inlet and interior vent configurations (#5-6), as shown in Figure 3, were considered. A simulation of flow front vs. time for port configurations #5 and #6 with a 1 mm gap are shown in Figure 5(b), and maximum fill time and final infusion outcome for each combination are provided in Table 1. Ultimately, configuration #5 (front inlet / central vent) was chosen for use in the VIPE bicycle seat tooling based on the simulation results and the simplicity of integrating a front inlet port compared to other locations.

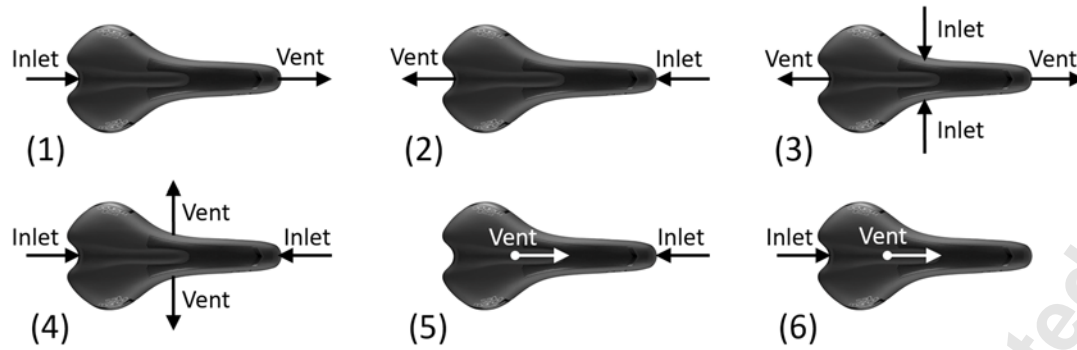


Figure 3. Resin inlet and vacuum vent port configurations considered for CFD simulation including (1) front vent / rear inlet, (2) front inlet / rear vent, (3) front & back vent / side inlet, (4) front & back inlet / side vent, (5) front inlet / central vent, and (6) rear inlet / central vent.

Table 1. Maximum fill times and resin fill behavior for the different resin inlet and vacuum vent configurations

Port Configuration	Edge Gap (mm)	Maximum Fill Time (s)	Infusion Details	Final Filling Result
1	0.1	1147	Slow infusion	Complete wet-out
	0.5	180	Rapid infusion	Large dry area
2	0.1	2392	Very slow infusion	Small dry area
	0.5	240	Medium infusion time	Medium dry area
3	0.1	521	Medium/slow infusion	Complete wet-out
	0.5	90	Very fast infusion	Very large dry area.
4	0.1	580	Medium/slow infusion	Small dry area
	0.5	77	Very fast infusion	Very large dry area
5	1	180	Rapid Infusion	Complete wet-out
	5	57	Very Rapid Infusion	Complete wet-out
6	1	133	Rapid Infusion	Complete wet-out
	5	54	Very Rapid Infusion	Complete wet-out

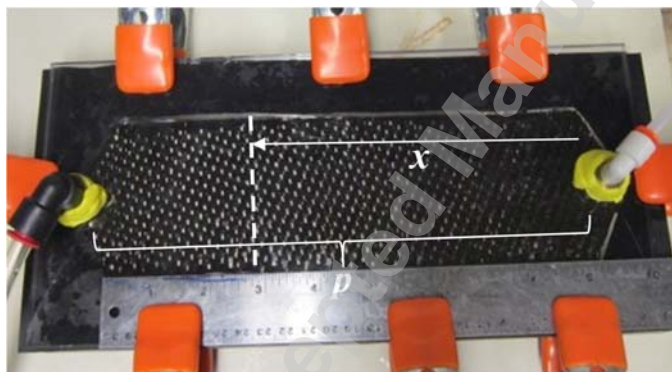
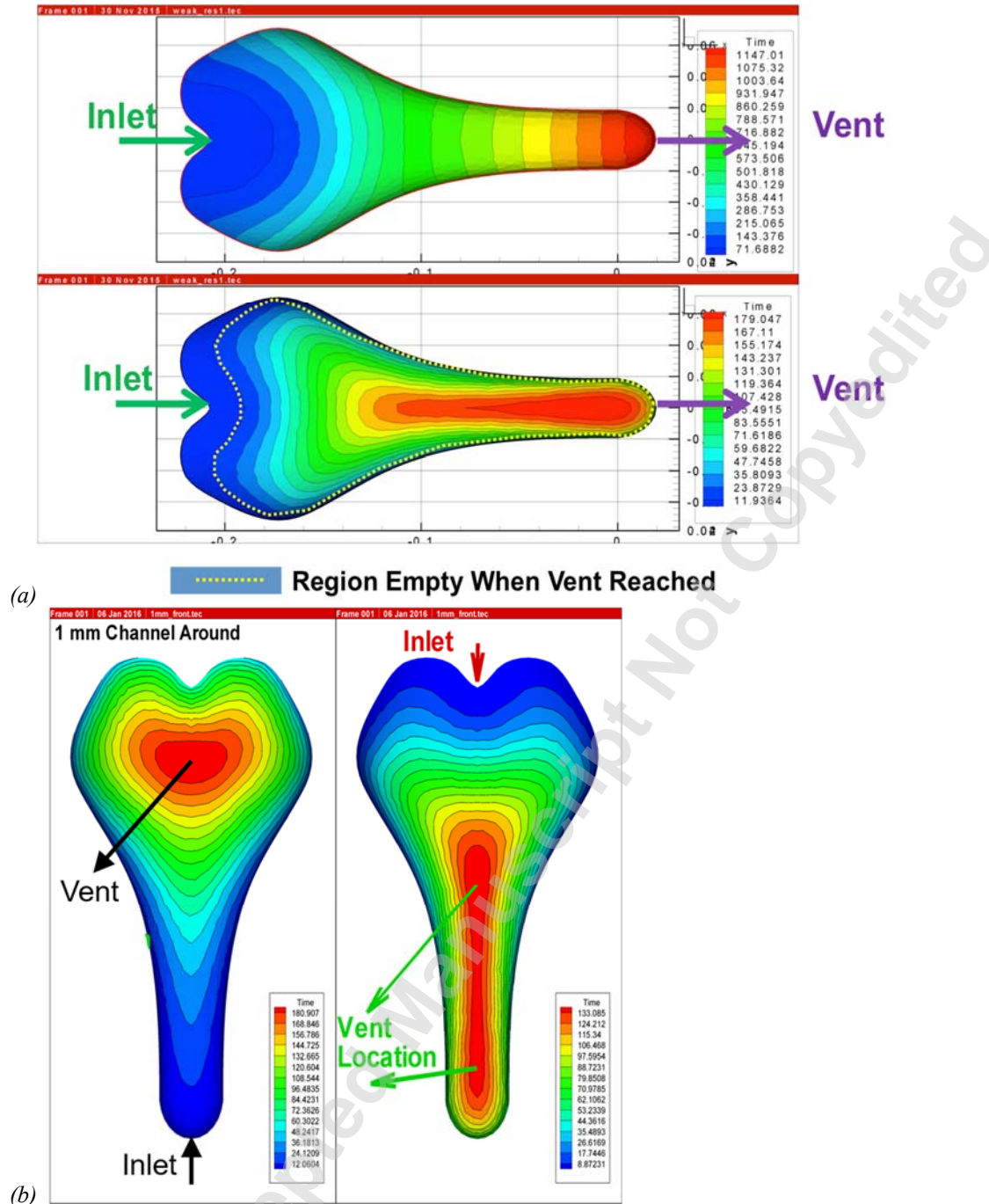


Figure 4. Unidirectional vacuum infusion testing apparatus for measuring permeability with flow front distance,  $x$ , and differential pressure,  $p$ , indicated.



(a) Figure 5. LIMS CFD models showing (a) port configuration #1 with 0.1 mm edge gap (top) and 0.5 mm edge gap (bottom) and (b) port configurations #5 (left) and #6 (right) with 1.0 mm edge gap.

### 3.2 Consolidation with Pressure Focusing Layer Tooling

A critical aspect of the VIPE process is design of the elastomeric mask and matching bottom mold used for PFL tooling. The elastomer chosen for the mask material is P-45 from Silicone, Inc, a 45 Shore A durometer, platinum-catalyzed silicone with a maximum working temperature of 316°C. A proprietary synthesis algorithm developed by Vistex Composites and structural modeling with Abaqus finite element analysis (FEA) software were used to iteratively design the desired mask shape. The FEA model consisted of quadrilateral hybrid elements to predict the

response of nearly incompressible materials such as silicone. A custom material model was used to capture the silicone's non-linear stress-strain relationship. Contact conditions at the aluminum mold/mask and mask/preform interfaces were based on frictional coefficients (Coulomb) measured experimentally. The iterative algorithm begins with a mask of uniform average thickness, the desired area to ultimately apply uniform consolidation pressure over, and the target pressure level applied to the composite part. The resulting pressure plot is used to drive geometry changes in simulation, and the process repeats until an acceptable pressure plot is achieved. In our case, convergence was achieved when the pressure distribution was within  $\pm 5\%$  of the target pressure. Pressure plots for a mask with uniform 12.7 mm starting thickness and final mask geometry after several iterations are shown in Figures 6(a) and 6(b), respectively. Notice how the pressure variation reduces from 1.5 MPa to 0.19 MPa. The final mask shape with variable thickness and a resin channel cut into the nose (based on port configuration #5 in Figure 3), and bottom PFL mold shapes are seen in Figure 7.

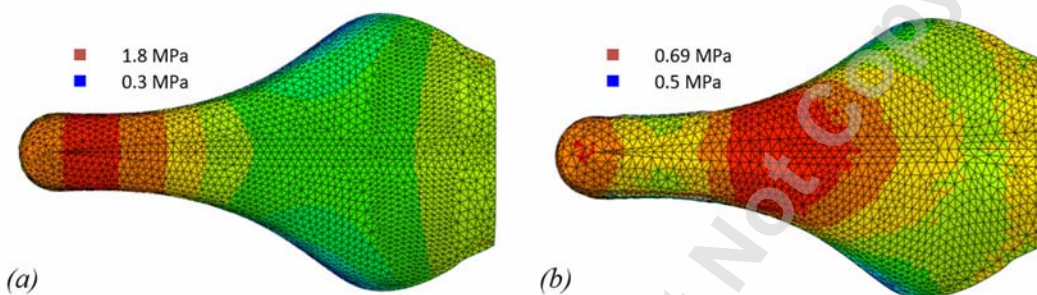


Figure 6. Elastomeric mask pressure plots for (a) first iteration and (b) final iteration.



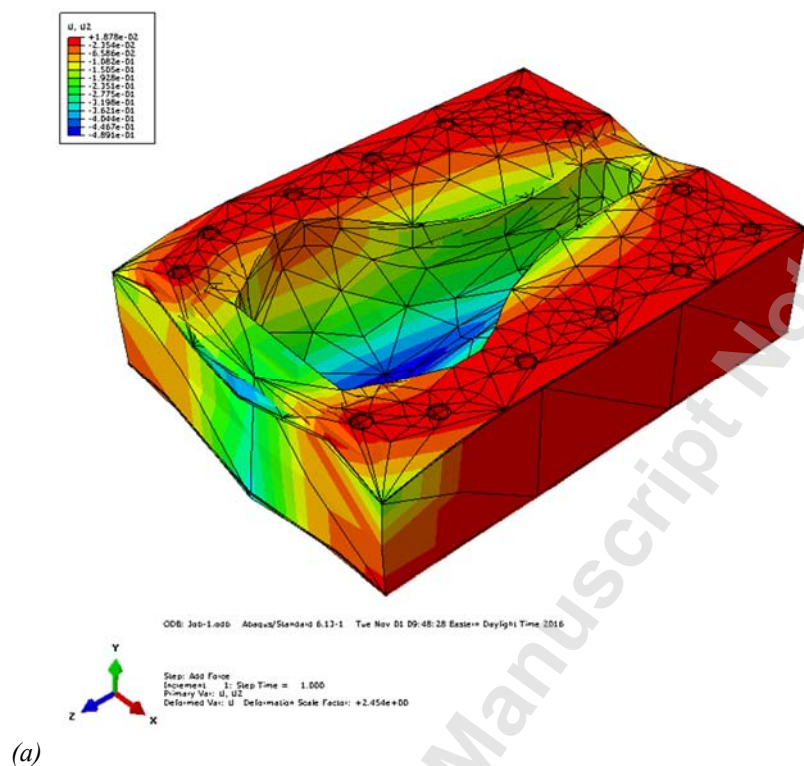
Figure 7. (a) Top (left) and bottom (right) views of the final elastomeric mask shape and (b) corresponding bottom mold shape.

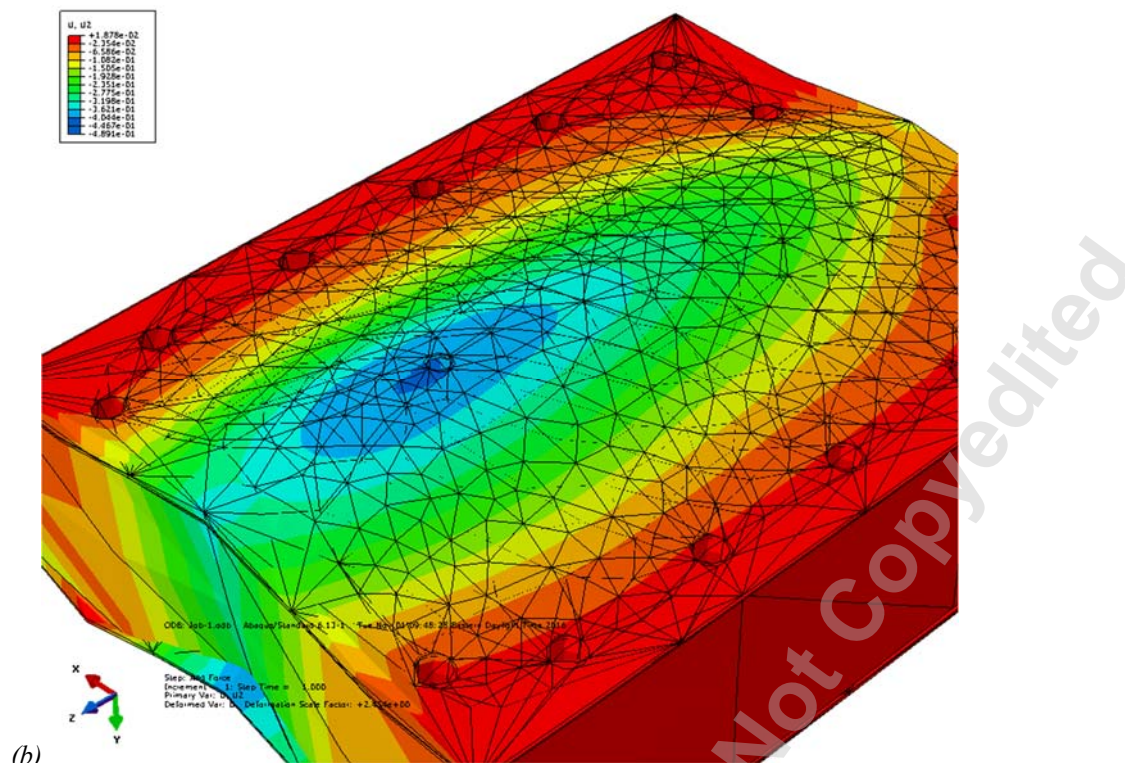
### 3.3 Top Mold Design

There were several important engineering specifications for the top mold including: (a) definition of the bicycle seat's A-side surface and final geometry, (b) incorporation of the resin inlet and vacuum venting ports, (c) maximum deflection not to exceed 0.5 mm after bolting the mold halves together and releasing clamping pressure, and (d) minimal electron beam attenuation during curing. A typical PFL top mold is designed to provide a uniform mold surface temperature and is fabricated out of aluminum by CNC machining. To avoid EB attenuation by the aluminum, the VIPE top mold is a composite sandwich construction consisting of laminate skins made of woven carbon fiber fabric (same as bicycle seat) impregnated with thermal-cure epoxy and a foam core.

FEA structural modeling using Abaqus was performed to determine the maximum deflection of the sandwich structure and engineer a final design that meets specifications. To simulate the

top mold when it is bolted under compression, the perimeter holes were modeled as fixed constraints and a 0.69 MPa pressure was applied to the inside mold surface. Material properties used were those for standard carbon fiber/epoxy laminates ( $E_1=160$  GPa,  $E_2=12$  GPa,  $G_{12}=4.4$  GPa,  $\nu_{12}=0.25$ ) in a  $[0,\pm 45]_s$  layup, which results in a bending stiffness matrix based on laminate theory of  $D = [380, 8.2, 0; 8.2, 82, 0; 0, 0, 12]$  GPa. To avoid having to machine rigid foam and for ease of fabrication, Fibre Glast 25/326 2 Lb. Polyurethane Mix and Pour Foam was used as the core material. Material properties for analysis were provided by the manufacturer ( $E=4.82$  MPa,  $\nu=0.3$ ). A final design consisting of 1.6 mm thick laminate skins and a 40 mm maximum thickness core resulted in a maximum predicted deflection of 0.49 mm near the venting port, as seen in Figure 8.





(b) Figure 8. FEA structural analysis of the top mold sandwich structure with (a) overall view of mold side and (b) close-up of maximum deflection on the exterior near the venting port.

Attenuation of the electron beam was analyzed at the thickest part of the sandwich structure core, where attenuation would be maximized, through Monte Carlo electron absorption simulations using CASINO simulation software. The laminates were modeled with a density of  $1.6 \text{ g/cm}^3$  (calculated using rule of mixtures) and thickness of  $1.6 \text{ mm}$ , while the core had a  $0.032 \text{ g/cm}^3$  density (from manufacturer) and  $40 \text{ mm}$  thickness. Simulations were conducted at three different electron energy levels –  $1.0$ ,  $2.0$ , and  $2.9 \text{ MeV}$  (maximum available from EB source) – and results (Figure 9) predicted that anything greater than  $2.0 \text{ MeV}$  allows electrons to fully penetrate the sample beneath the sandwich structure tooling.

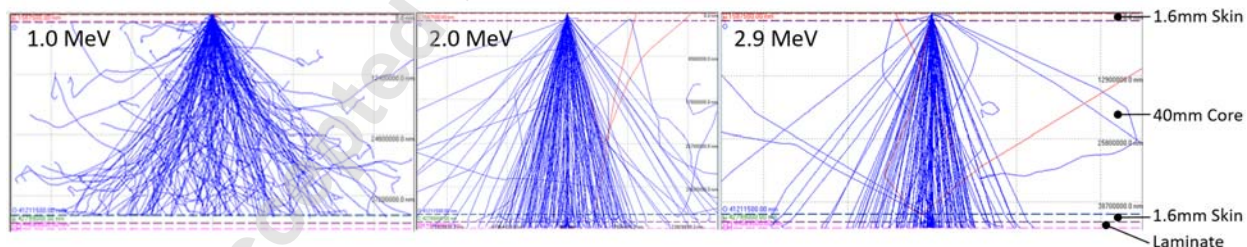


Figure 9. EB electron penetration simulations for (a)  $1.0 \text{ MeV}$ , (b)  $2.0 \text{ MeV}$ , (c)  $2.9 \text{ MeV}$  energies.

### 3.4 Final Tooling Design

The final CAD geometry of the VIPE bicycle seat tooling is shown in Figure 10. The bottom aluminum mold (aka compression mold), consisting of a shape machined using a Computer Numerically Controlled (CNC) 3-axis milling machine bolted to a base plate, defines the required geometry that backs the mask during compression to provide uniform consolidation pressure. The seat shape is raised vertically more than is necessary for the VIPE process to allow

it to be clamped in a vise during CNC machining. An aluminum spacer plate is required to compensate for this extra height during part production and has perimeter channel to accommodate a  $\varnothing 3.2$  mm O-ring for sealing during resin infusion. The spacer also has a through hole from the side edge to the nose of the seat that serves as the resin inlet port. The PFL mask covers the bottom mold and seals the spacer plate/mold interface from resin leakage. A dry laminate preform (manufacturing details provided later in Section 4.2) is placed on top of the mask and is covered by the top mold made of a sandwich construction. Finally, the entire assembly is held together with a series of clamping bolts.

The next section discusses fabrication of the tooling itself and manufacturing of composite parts using this tooling.

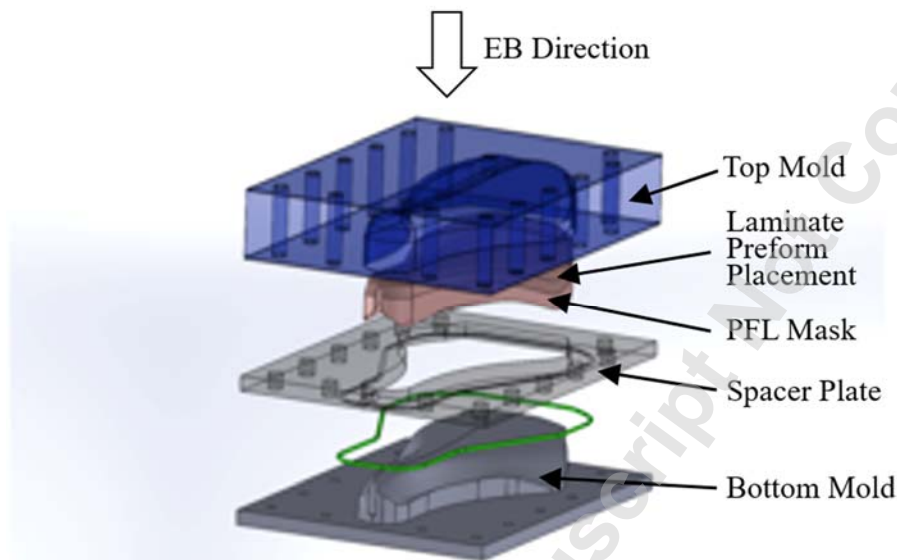


Figure 10. Exploded view of VIPE bicycle seat mold

## 4. Tooling and Composite Part Fabrication

### 4.1 Tooling Fabrication

The bottom mold components – a 12.7 mm-thick backing plate and a bicycle seat shape – were CNC machined out of 6061 Aluminum and bolted together into a unitized assembly. The spacer was similarly CNC-machined out of 6061 Aluminum and then epoxied to the backing plate with its O-ring channel facing upwards, as shown in Figure 11.

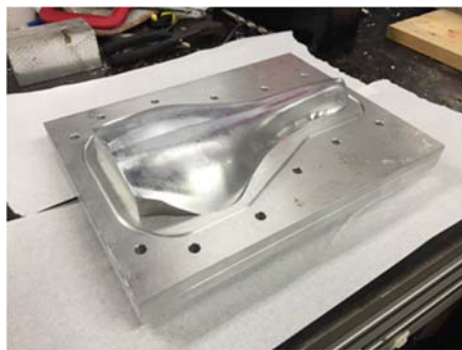


Figure 11. Bottom mold/spacer plate assembly

The top mold was fabricated manually in-house due to the complex shape and sandwich construction. The top laminate skin and bottom laminate skin (see Figure 12(a)) were made using a wet-layup process, wherein the textile plies were cut, hand impregnated with resin and laid up on a mold, vacuum bagged (including release layer and breather cloth), consolidated at 0.91 kPa of vacuum, and allowed to cure under a heat lamp. The top skin mold was simply a polished aluminum plate, whereas bottom skin mold was machined from aluminum mold the exact shape of the seat's exterior A-side (top) surface. To create a mold for the sandwich construction, the top laminate skin was mated with a polyurethane tooling frame that was the required thickness, as shown in Figure 12(b). The foam core material was mixed and poured over the laminate, the bottom laminate was placed on top of the foam, and an aluminum plate was placed over top of the walls to prevent the foam from lifting the top laminate skin above the desired thickness. After letting the foam cure for 10 minutes, the top mold (Figure 12(c)) was extracted from the frame. Through holes for the bolts were machined later.



Figure 12. (a) bottom laminate skin, (b) pouring mold for mix-and-pour foam core, and (c) final top mold construction.

The PFL mask was made using the VIPE bottom mold assembly and top mold to create the casting cavity. The RTV silicone, a 2-part, mix-and-pour style elastomer, was mixed together by hand, degassed in a vacuum chamber, and poured into the mold. To accommodate the actual part thickness, silicone sheet of the desired thickness was cut to the same shape as the fiber preform and laid over the bottom mold to serve as the offset. The mask silicone was poured on top of the offset mask, and the molds were closed using a standard lab press (Figure 13(a), allowing the excess silicone to squeeze out around the edges. As the RTV silicone vulcanized at room temperature, it was left overnight (12 hours) for the mask to solidify. The mask (red) with offset sheet (gray) and final mask are shown in Figures 13(b) and 13(c), respectively.

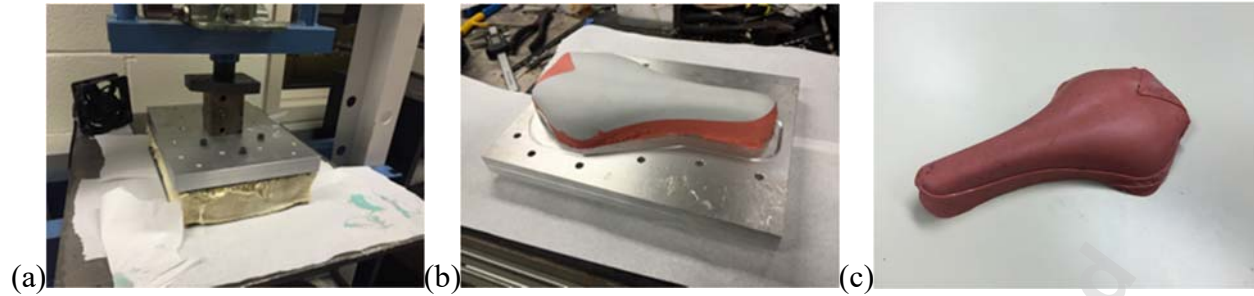


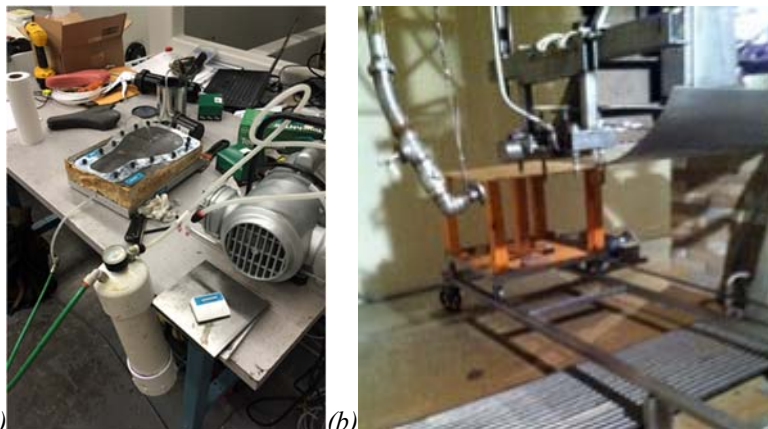
Figure 13. (a) PFL mask curing using the VIPE top and bottom molds, (b) mask with offset sheet after vulcanization, and (c) final mask.

## 4.2 Part Fabrication

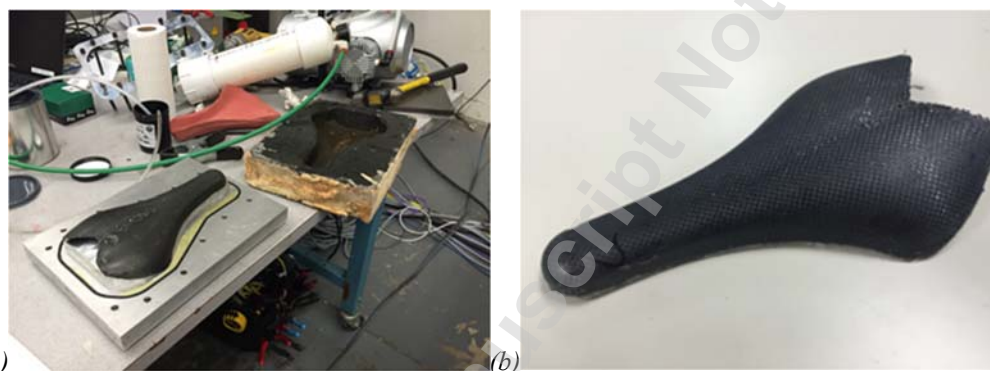
Fabrication of bicycle seats using the VIPE process is a multi-step process with details provided below.

- A. Individual woven carbon plies were cut without frayed edges to the required preform shape using an Epilog 50 Watt laser cutter. Cutting took about 30 s per ply.
- B. The molding surfaces (bottom mold, PFL mask) were coated with mold release agent appropriate for an epoxy acrylate resin.
- C. The required number of plies (4 or 5) were laid in the correct position in the top mold flipped over, and then covered by the bottom mold assembly with PFL mask and O-ring.
- D. Infusion of the EB-curable resin required running plastic tubing from the resin pot to the mold inlet port then from the mold outlet through a resin trap to a high-vacuum pump (Figure 14(a)). A maximum vacuum level of 91 kPa was maintained during infusion for all specimens, and resin was observed entering the catch pot after approximately 3 min in each case. Following infusion, a 5 mm-thick silicone plug was placed in the central vacuum venting port to close the mold, since tubing would interfere with the compression and curing step.
- E. A hydraulic shop press was used to apply the required 19.5 kN load over the bicycle seat's projected 0.0282 m<sup>2</sup> surface area to achieve the 0.69 MPa consolidation pressure. Clamping bolts were tightened until they were snug to maintain the pressure, and then the ram load was released.
- F. Part irradiation and curing occurred at IBA Industrial (Edgewood, NY, USA), a manufacturer of industrial-scale EB equipment, using their 3.0 MeV E-Beam machine, shown in Figure 14(b). This machine has a 2.5×91 cm beam window and conveyor system with coordinated velocity to provide a consistent radiation dose to the workpiece (Figure 14(c)). During processing, the top mold was facing upwards towards the accelerator beneath the EB window. The cationic resin required four 20 kGy passes to achieve the maximum 80 kGy dose suggested by the manufacturer. Total exposure time per part was approximately 30-40 sec. It should be noted that only 1/6<sup>th</sup> of the accelerator's beam window was used for actual part curing, so multiple parts could have been cured at the same time.
- G. After irradiation and removal from the EB accelerator's concrete chamber, clamping bolts on the VIPE tool were loosened and the molds separated. A knockout pin was placed in center port and rapped with a mallet to dislodge the part. The mold surface was cleaned of any uncured resin and mold release was reapplied after every five parts. Images of the

separated molds and a typical part after removal are shown in Figure 15. No further processing was done to the part (e.g., edge trimming). The total number of bicycle seats produced depended entirely on the limited amount of time available at the EB facility. Hence, ten parts were produced – five 4-ply laminates and five 5-ply laminates. The extra ply was added to see how this would affect part performance and quality.



(a) (b)  
Figure 14. Images of (a) the resin infusion step and (b) the 3MeV EB accelerator and conveyor system.



(a) (b)  
Figure 15. (a) Finished part after removal from mold and (b) top view of a typical untrimmed bicycle seat.

## 5. Experimental Results and Discussion

### 5.1 Part Thickness

Thickness measurements were taken at five different locations on each saddle, as indicated in Figure 16(a), using a Mitutoyo IP-65 deep throat ball caliper. The ball helps to alleviate issues in measuring the thickness of curved surfaces. Results of the average thickness for all five locations, provided in Table 2, indicate that the laminates are sufficiently consolidated after resin infusion. Interestingly, consolidation of the 4-ply parts is greater than that of the 5-ply parts. For a grand average 4-ply thickness of 0.92 mm, we would expect the 5-ply to be 20% thicker, i.e.  $1.2 \times 0.92 \text{ mm} = 1.11 \text{ mm}$ . Instead, the grand average 5-ply thickness is 1.26 mm.

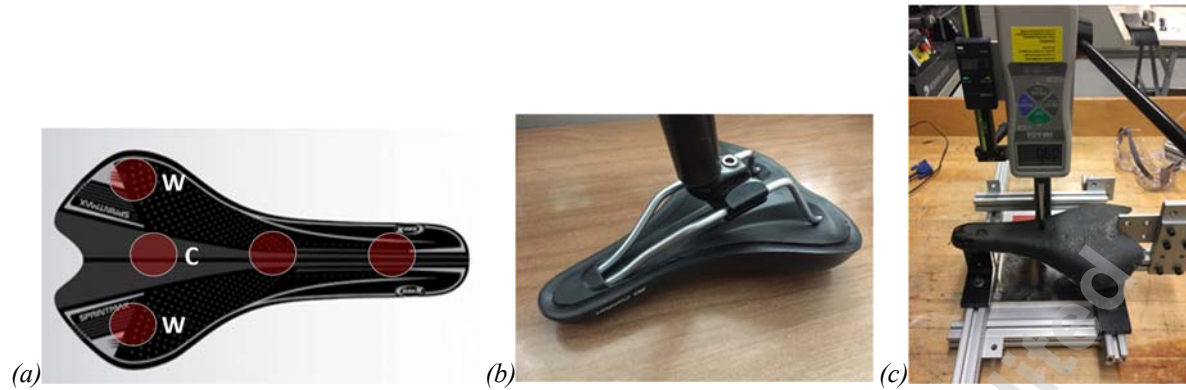


Figure 16. (a) Locations for part thickness and volume fraction measurements, (b) support rails for bicycle seat, and (c) seat stiffness test rig with seat mounted for testing.

Table 2. Bicycle seat thickness, stiffness, and surface roughness results

Part #	# of Plies	Thickness (mm)		Part Stiffness (N/mm)		Surface Roughness ( $\mu\text{m}$ )			
		Avg.	$\sigma$	Avg.	$\sigma$	$R_a$		$S_a$	
						Avg.	$\sigma$	Avg.	$\sigma$
1	4	0.93	0.05	37.6	0.5	2.17	1.06	2.12	0.90
2		0.84	0.03	29.7	0.2	1.77	0.74	1.93	0.72
3		0.86	0.03	35.1	0.3	1.79	0.73	1.66	0.67
4		0.98	0.06	36.9	0.3	1.89	0.54	1.89	0.74
5		1.01	0.08	44.5	0.5	2.01	0.70	1.76	0.90
6	5	1.24	0.05	51.3	0.6	2.43	1.43	2.03	0.98
7		1.29	0.09	56.4	1.0	3.31	2.46	2.19	1.26
8		1.23	0.06	58.0	1.5	2.27	1.51	1.70	0.85
9		1.24	0.08	71.4	1.4	2.33	1.41	2.14	1.58
10		1.32	0.05	76.2	2.2	1.25	0.81	1.34	0.61

## 5.2 Part Stiffness

Part stiffness was measured by supporting the bicycle seat similar to an actual mount, subjecting the part to a centrally located load of 5, 10, or 15 kgf (49, 98 & 147 N) loads, and measuring the corresponding deflection beneath the load point. Although the specific stiffness measured is not of any particular structural significance, it does allow for mechanical performance comparisons between parts. As shown in Figure 16(b), a custom-designed test rig, consisting of a three support points based on dimensions of the seat rails and a registration plate for the seat's rear V-notch, was used as a seat fixture during deflection tests. Force and deflection were applied and measured, respectively, using an Imada NLV-220-C compression test stand. Part stiffness results (see Table 2) indicate that part stiffness increases with the number of plies, as expected, and there is significant variation in measured stiffness among similar parts.

## 5.3 Surface Roughness – $R_a$ and $S_a$

Arithmetic mean roughness, both linear ( $R_a$ ) and area ( $S_a$ ), were measured for all 10 parts using an Alicona InfiniteFocus optical surface profiler, and results are provided in Table 2. Measurements were taken at six locations on each part including the nose, the center, and one of the wings for both the top (A-side) and bottom (B-side) sides, although obvious surface voids were excluded. Grand average  $R_a$  for the 4-ply and 5-ply parts were similar (1.93 vs. 2.32  $\mu\text{m}$ , respectively) and fall within the ISO N8-N9 surface grades. Likewise, values of  $S_a$  for the 4-ply

and 5-ply parts were similar (1.87 vs. 1.88  $\mu\text{m}$ , respectively). Winger et al. [30] has shown that the composite takes on the surface roughness of the tool surface. Hence, the relatively rough surface finishes for parts on the A-side reflect the rough top mold surface.

#### 5.4 Volume Fractions

Relatively flat specimens from the center and wing sections (indicated by *C* and *W* in Figure 16(a), respectively) of Parts 1, 3, 5, 6 and 9 were tested for fiber, matrix, and void volume using Test Method I (acid digestion) in ASTM D3171. This method involves exposing the laminate to an acid to dissolve away the polymer matrix surrounding the fibers, then cleaning, drying, and weighing the fibers. If the weights and dimensions of the initial specimens, as well as the densities of the reinforcement and matrix ( $\rho_{cf} = 1.84 \text{ g/cm}^3$ ,  $\rho_{epoxy} = 1.1 \text{ g/cm}^3$ ) are known, the fiber ( $V_f$ ), matrix ( $V_m$ ), and void ( $V_v$ ) volume fractions can be determined.

Inter-part and intra-part volume fraction values varied significantly, as shown in Figure 17. Within the 4-ply group (1, 3 and 5),  $V_f$  varied from 41.7 to 62.2% and  $V_v$  from 0 to 6.9%. There was little intra-part repeatability. Within the 5-ply group (6 and 9),  $V_f$  varied from 33.8 to 53.1% and  $V_v$  from 0 to 3.4%. Part 9 had the most repeatable volume fraction values of all five parts measured, whereas Part 6 was the most resin rich ( $V_m \sim 70\%$  for both locations) and, accordingly, had the lowest part stiffness (see Table 2) within that group. Part stiffness and fiber volume fraction of the five parts is provided in Table 3. Interestingly, higher  $V_f$  clearly results in higher part stiffness for the 5-ply parts measured, but there is essentially no correlation with the 4-ply parts. The high variation in volume fractions is not surprising given the limited number of parts produced and proof-of-concept objective for the experimental work.

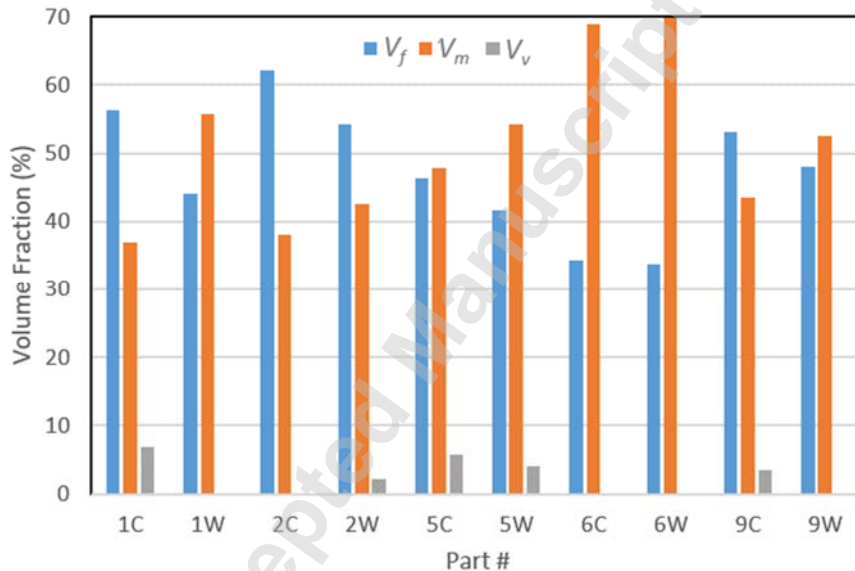


Figure 17. Fiber, matrix, and void volume fractions for select VIPE parts

Table 3. Part stiffness vs.  $V_f$

Part #	# of Plies	Stiffness (N/mm)	$V_f$ (%)
1	4	37.6	50
2		29.7	58
5		44.5	44
6	5	51.3	34

9		71.4	51
---	--	------	----

## 5.5 Discussion

As expected, part thickness in Table 2 generally corresponds to the number of plies. However, there is significant thickness and stiffness variation among the 10 parts as reflected in average values and standard deviation. Part surface roughness is largely dependent on finish of the top mold's skin. Fiber volume and matrix fractions varied significantly and ran the gamut from aerospace quality (Part #2) to what would be considered a low-quality composite component (Part #6).

Some of the variation observed in part thickness, stiffness, surface roughness, and fiber and matrix volume fractions is attributable to changes in condition of the VIPE tooling. First, properties of the core material used in the sandwich structure were degraded by the EB irradiation, most notably after the first cure dose (80 kGy). After bolting the mold-set together for the second saddle compression step, significant geometrical distortion and discoloration was observed in the top mold (Figure 18(a)) as compared to a virgin mold (Figure 18(b)). Second, vacuum sealing may have been compromised during resin infusion leading to some resin-starved areas in some parts (Figure 19(a)). Third, the top mold surface delaminated in a number of locations by what is believed to be trapped moisture in large voids within that matrix that expanded during material heat-up during EB irradiation (Figure 19(b)). The resin used for the top skin was not degassed before layup, although it was cured in a vacuum bag.

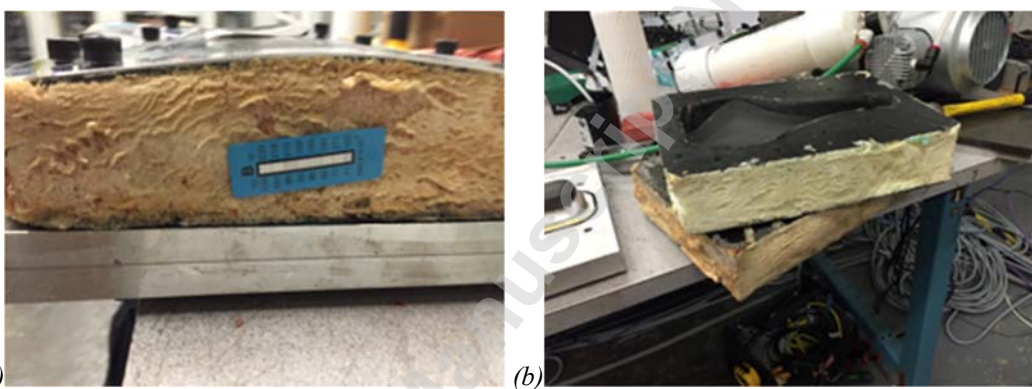


Figure 18. (a) Irradiated sandwich structure under compression, (b) virgin sandwich structure on top of irradiated sandwich structure

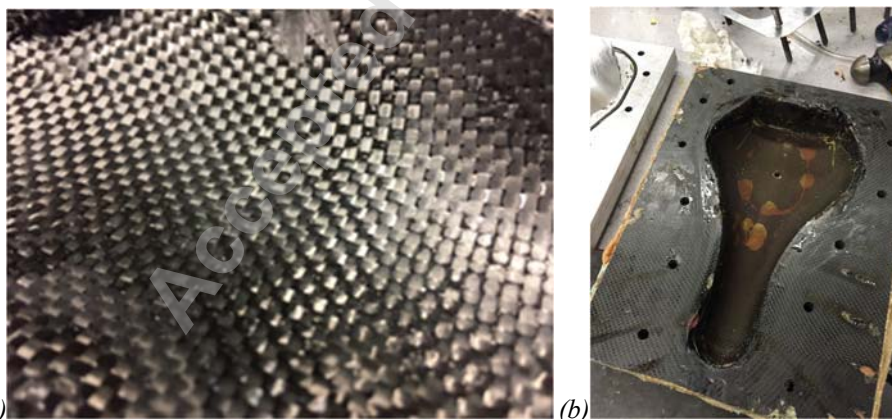


Figure 19. Views of (a) resin-starved region close-up and (b) delaminated spots of top mold surface.

## 6. Conclusions and Future Work

The VIPE process has been successfully applied to a complex, industrially relevant 3-D part shape, specifically a 4-5 ply woven carbon/epoxy bicycle seat. The key to demonstration of this process technology was innovative design, engineering, and fabrication of a tool that can accommodate vacuum infusion, out-of-autoclave consolidation, and electron beam curing. The design process began with CFD simulations of a dry fiber preform based on experimental characterization of permeability for the chosen reinforcement/resin combination. Different resin inlet and vacuum venting configurations were simulated to identify the best one for minimizing both infusion time and the risk of incomplete wet-out. The next step was design of the PFL mold (silicone mask backed by a rigid aluminum mold) to provide uniform consolidation pressure using iterative finite element (FE) structural analysis and a proprietary algorithm. Finally, the stiff, EB-transparent top mold was designed (i.e. materials and geometry specified) using static FE analysis and Monte Carlo electron absorption simulations. CNC machining of the bottom mold and casting of the PFL mask were straightforward tasks. The real challenge was in fabricating the top mold. The tool-side skin required a separate polished mold, wet layup operation, and room-temperature cure. After the cured lower skin was enclosed by a box structure, the castable foam core material was poured and capped with the flat upper skin. Only 10 composite parts were made due to limited access to a high energy EB accelerator.

Characterization of composite parts produced using the VIPE tooling and process provide two important findings: (1) rapid manufacturing of high quality parts is possible (cycle time < 1 min,  $V_f \sim 60\%$ ,  $V_v \sim 0\%$ , repeatable surface finish) and (2) quality characteristic variability is quite high. The latter finding is primarily attributable to fabrication and material issues with the top mold subjected to the extreme EB irradiation conditions and also the limited number of parts produced. It is unclear if the top mold damage was caused exclusively from heating due to EB or from the EB itself, but the damage significantly affected compression of the mold. The mold surface also suffered from blistering and cracking due to trapped gases in sub-surface voids heating and expanding. The damaged core led to some over-compression and lack of vacuum during compression, causing incomplete wet-out in some latter parts.

Several areas of future work need to be pursued to determine full market viability of the VIPE process. First of all, a complex 3-D geometry part needs to be produced in large enough quantities as part of a designed experiment to perform objective quality analysis, correlate input parameters to output variables, and perform sensitivity analyses without experiencing the same top mold issues as described in this paper. The use of higher quality core material (e.g., CNC-machined honeycomb core), as well as industry-standard production methods for making the mold will work towards this goal. The mold integrity is the most important aspect of this research for accurately applying and maintaining the desired compression on the parts. After completion of an undamaged production mold, full lifecycle analysis of VIPE tooling must be conducted with a particular focus on integrity of the sandwich structure and the elastomeric mask. Degree of cure experiments should also be completed with the VIPE process in mind to confirm that parts are being fully cured. In addition, a working manufacturing cell should be implemented in an EB facility to analyze the cycle time and economic pros and cons of this approach.

## 7. Acknowledgements

The authors would like to acknowledge several organizations for their support of this research work including the National Science Foundation through Grant No. 1200847, the New York State Energy Research Development Authority (NYSERDA) through Grant #43683,

Rensselaer's Center for Automation Technologies and Systems (CATS), Vistex Composites, LLC, Rapid Cure Technologies, Inc., and IBA Industrial, Inc.

## 8. References

- [1] Global Thermoset Composites Industry, Report # 6033124, Global Industry Analysts, Inc., April 2021.
- [2] Beziers D, Perilleux P and Grenie Y. Composite structures obtained by ionization curing. *Radiat Phys Chem* 1996; 48(2): 171–177.
- [3] Crasto AS, Kim R, Rice BP, Electron Beam Cure of Composites for Aerospace Structures, Proceedings of ICCM-11, Gold Coast, Australia, July 14-18, 1997, pp.IV-271-278.
- [4] Lopata VJ, Saunders CB, Singh A, Janke CJ, Wrenn GE, Havens SJ, 1999, Electron-beam-curable epoxy resins for the manufacture of high-performance composites, *Radiat. Phys. Chem.*, 56, pp.405-416.
- [5] Glauser T, Johansson M, Hult A, 2000, A comparison of radiation and thermal curing of thick composites, *Macromol. Mater. Eng.*, 274, pp.25–30.
- [6] Berejka AJ, Eberle C, 2002, Electron beam curing of composites in North America, *Radiat. Phys. Chem.*, 63, pp.551-556.
- [7] Lopata VJ, Sidwell DR, 2003, Electron Beam Processing for Composite Manufacturing and Repair, Sept./Oct. 2003, pp.32-42.
- [8] Zsigmond B, Halasz L, Czvikovszky T, 2003, Electron beam processing of carbon fibre reinforced braided composites, *Radiat. Phys. Chem.*, 67, pp.441-445.
- [9] Nishitsuji DA, Marinucci G, Evora MC, Silva LGA, 2010, Cationic concentration effects on electron beam cured of carbon-epoxy composites, *Radiat. Phys. Chem.*, 79, pp.306-309.
- [10] Vautard F, Ozcan S, Poland L, Nardin M, Meyer H, 2013, Influence of thermal history on the mechanical properties of carbon fiber-acrylate composites cured by electron beam and thermal processes, *Compos. Part A Appl. Sci. Manuf.*, 45, pp.162-172.
- [11] Chappas WJ, Devney BG, Olding RP, McLaughlin WL, 1999, EB curing of maritime composite structures, *Radiat. Phys. Chem.*, 56, pp.417-427.
- [12] Saunder C, Lopata V, Barnard J, Stepanik T, 2000, Electron beam curing – taking good ideas to the manufacturing floor, *Radiat. Phys. Chem.*, 57, pp.441-445.
- [13] Jianwen B, Fengmei L, Yang L, 2000, Study on the Heat-Resistant EB Curing Composites, Proceedings of JAERI-Conf 2000-001, Oct. 25-29, 1999, Kyoto, Japan, pp.235-38.
- [14] Coqueret X, Krzeminski M, Ponsaud P, Defoort B, 2009, Recent advances in electron-beam curing of carbon fiber-reinforced composites, *Radiat. Phys. Chem.*, 78, pp.557-561.
- [15] Vautard F, Grappe H, Ozcan S, 2014, Engineering Interface Chemistry to Improve the Strength of Carbon Fiber Composites Cured by Electron Beam, *Ind. Eng. Chem. Res.*, 53, pp.12729-12736.
- [16] Zhang J, Duan Y, Wang B, Zhang X, 2020, Interfacial enhancement for carbon fibre reinforced electron beam cured polymer composite by microwave irradiation, *Polymer*, 192, 122327 (11 pages).
- [17] Goodman DL, Byrne CA, Yen A, Moulton R, Dixon D, Costen RC, 1999, Automated Tape Placement With In-Situ Electron Beam Cure, International SAMPE Symposium, 44, p.269.
- [18] Fengmei L, Jianwen B, Xiangbao C, Huaying B, Huiliang W, 2002, Factors influencing EB curing of epoxy matrix, *Radiat. Phys. Chem.*, 63, pp.557-561.
- [19] Sui G, Zhang Z, Liang Z and Chen C. Dynamic Mechanical Studies on Epoxy Resins Cured by Electron Beam Radiation. *Mater Sci Eng* 2003; 342(1-2): 28-37.

- [20] Abliz D, Duan Y, Zhao X, Li D, 2014, Low-energy electron beam cured tape placement for out-of-autoclave fabrication of advanced polymer composites, *Compos. Part A Appl. Sci. Manuf.*, 65, pp.73-82.
- [21] Walczyk, D., Hoffman, C., Righi, M., De, S. and Kupperts, J., “Consolidating and Curing of Thermoset Composite Parts by Pressing Between a Heated Rigid Mold and Customized Rubber-Faced Mold,” U.S. Patent 8,511,362, Issued on Aug. 20, 2013.
- [22] <https://www.vistexcomposites.com/technology>
- [23] Walczyk, D., Kupperts, J. and Hoffman, C., “Curing and Consolidation of Advanced Thermoset Composite Laminate Parts by Pressing Between a Heated Mold and Customized Rubber-Faced Mold,” *J. Manuf. Sci. Eng.*, 133(1), February 2011, 011002 (7 pages).
- [24] Walczyk, D. and Kupperts, J., “Thermal press curing of advanced thermoset composite laminate parts,” *Composites Part A*, 43(4), 2012, pp. 635–646.
- [25] Kupperts, J. and Walczyk, D., “Refinement of the Thermal Press Curing Process for Advanced Composites,” *Journal of Manufacturing Science and Engineering*, 136(2), April 2014, pp.021014 (12 pages).
- [26] Malek, P. and Walczyk, D., “Silicone Rubber Properties During Consolidation/Curing of Advanced Composites using Specialized Elastomeric Tooling (SET),” *Journal of Manufacturing Science and Engineering*, 138(2), Feb. 2016, 021002 (7 pages).
- [27] Garofalo, J., Walczyk, D. and Kupperts, J., “Rapid Consolidation and Curing of Vacuum-Infused Thermoset Composite Parts,” *J. Manuf. Sci. Eng.*, 139(2), Sept. 2016, 201021010 (10 pages).
- [28] Garofalo, J., Walczyk, D. and Bucinell, R., “Low-Cost Manufacturing and Recycling of Advanced Biocomposites,” *Journal of Natural Fibers*, 16(3), 2019, pp. 412-426.
- [29] Rizzolo, R., Walczyk, D., Kupperts, J., Montoney, D. and Galloway, R., “Rapid Consolidation and Curing of Advanced Composites Using Electron Beam Irradiation,” *Journal of Engineering Manufacture*, 233(4), March 2019, pp. 1168-1181.
- [30] Wenger, W., Dickson, G.R., McIlhagger, R., and Miller, P.P., “The surface-finish characteristics of composite components,” *Journal of Materials Processing Technology*, 33, 1992, pp. 439-452.